

Solar wind parameters influencing magnetosheath jet formation: low and high IMF cone angle regimes

Laura Vuorinen¹, Heli Hietala^{1,2,3}, Adrian T. LaMoury², and Ferdinand Plaschke⁴

¹Department of Physics and Astronomy, University of Turku

²Blackett Laboratory, Imperial College London

³Department of Physics and Astronomy, Queen Mary University of London

⁴Institut für Geophysik und extraterrestrische Physik, TU Braunschweig

June 25, 2023

Solar wind parameters influencing magnetosheath jet formation: low and high IMF cone angle regimes

Laura Vuorinen¹, Heli Hietala^{1,2,3}, Adrian T. LaMoury², and Ferdinand Plaschke⁴

¹Department of Physics and Astronomy, University of Turku, Turku, Finland

²Blackett Laboratory, Imperial College London, London, United Kingdom

³Department of Physics and Astronomy, Queen Mary University of London, London, United Kingdom

⁴Institut für Geophysik und extraterrestrische Physik, TU Braunschweig, Braunschweig, Germany

Key Points:

- Jet formation is sensitive to SW parameters during high IMF cone angles (quasi- \perp), but not during low cone angles (quasi- \parallel)
- Quasi- \parallel (quasi- \perp) jets have an intrinsic size of $\sim 0.3 R_E$ ($\sim 0.1 R_E$) parallel to flow
- Quasi- \perp jet formation is related to shock dynamics amplified by higher β and M_A

Corresponding author: Laura Vuorinen, laura.k.vuorinen@utu.fi

Abstract

Magnetosheath jets are localized flows of enhanced dynamic pressure that are frequently observed downstream of the Earth’s bow shock. They are significantly more likely to occur downstream of the quasi-parallel shock than the quasi-perpendicular shock. However, as the quasi-perpendicular geometry is a more common configuration at the Earth’s subsolar bow shock, quasi-perpendicular jets comprise a significant fraction of the observed jets. We study the influence of solar wind conditions on jet formation by looking separately at jets during low and high interplanetary magnetic field (IMF) cone angles. According to our results, jet formation commences when Alfvén Mach number $M_A \gtrsim 5$. We find that during low IMF cone angles (downstream of the quasi-parallel shock) other solar wind parameters do not influence jet occurrence. However, during high IMF cone angles (downstream of the quasi-perpendicular shock) jet occurrence is higher during low IMF magnitude, low density, high plasma beta (β), and high M_A conditions. The distribution of quasi-parallel (quasi-perpendicular) jet sizes parallel to flow peaks at $\sim 0.3 R_E$ ($\sim 0.1 R_E$). Some quasi-perpendicular jets formed during high β and M_A are particularly small. We show examples of quasi-perpendicular shock crossings to better understand the influence of β and M_A conditions on jet observations. Our results suggest that jets form as part of the quasi-perpendicular shock dynamics amplified by high solar wind M_A and β . Such jets seem to be observed in the transition region of the shock, but not deeper in the magnetosheath.

1 Introduction

Magnetosheath jets are dynamic pressure enhancements that sporadically emerge from the Earth’s bow shock and are then observed in the magnetosheath (see the review by Plaschke et al., 2018, and the references therein). These are very common structures as one satellite can observe them many times per hour. Their sizes vary with the largest ones being comparable to the size of the Earth (Plaschke et al., 2016, 2020). Many studies have linked jets to low interplanetary magnetic field (IMF) cone angle (the acute angle between the Sun-Earth line and the magnetic field) conditions (e.g., Archer & Horbury, 2013; Plaschke et al., 2013; Vuorinen et al., 2019; LaMoury et al., 2021). At the subsolar magnetosheath, the cone angle approximates the nominal θ_{Bn} at the bow shock, as the curvature of the shock is small in this region. Thus, these results imply that jets are most frequent when the subsolar magnetosheath is downstream of a quasi-parallel bow shock region.

This trend in jet occurrence has implications for jet formation mechanisms — namely that they are most likely related to the nature of the quasi-parallel shock and to the presence of the foreshock. For example, foreshock transients such as short large amplitude structures (SLAMS; Schwartz, 1991) or foreshock compressive structures (FCS) in general can pass through the bow shock and be observed as dynamic pressure enhancements in the magnetosheath (Karlsson et al., 2015; Palmroth et al., 2018; Suni et al., 2021). In addition, Hietala et al. (2009) and Hietala and Plaschke (2013) argued that jets can emerge from a rippled quasi-parallel shock surface, when solar wind flowing through a ripple is less decelerated than the flow through the surrounding shock area. Recently, Raptis et al. (2022) showed direct evidence of a jet forming during the reformation process of the quasi-parallel shock, as solar wind was trapped downstream between the old and newly-forming shock surface. A minority of jets can also be attributed to solar wind discontinuities interacting with the Earth’s bow shock (Archer et al., 2012).

A non-negligible fraction of jets do occur during high IMF cone angles downstream of the quasi-perpendicular shock. The quasi-perpendicular geometry is in fact a much more common configuration for the subsolar bow shock (see Figure 1a introduced in Section 2). This results in the number of jets downstream of quasi-parallel and quasi-perpendicular shocks being more comparable in data sets consisting of many years of dayside magne-

66 tosheath observations (see Figure 1). Interplanetary shocks at 1 AU and planetary bow
 67 shocks beyond Earth are also frequently quasi-perpendicular. More attention has been
 68 recently paid to these jets in the quasi-perpendicular magnetosheath. Raptis et al. (2020)
 69 studied jets (enhancements of total dynamic pressure) in the quasi-perpendicular mag-
 70 netosheath along with quasi-parallel and boundary jets (between the two regimes). They
 71 divided these jets downstream of the quasi-perpendicular shock into two categories: quasi-
 72 perpendicular jets and encapsulated jets (jets which look like quasi-parallel jets but are
 73 observed in the quasi-perpendicular magnetosheath). They argued that encapsulated jets
 74 are most likely formed at the quasi-parallel shock but they travel in the magnetosheath
 75 and can later be observed in the quasi-perpendicular region. Raptis et al. (2020) found
 76 quasi-perpendicular jets to be shorter in duration and weaker in speed, density, and dy-
 77 namic pressure. Kajdič et al. (2021) studied total dynamic pressure enhancements in the
 78 quasi-perpendicular magnetosheath and reported four different types of events, which
 79 resulted in jet-like enhancements: reconnection exhausts, magnetic flux tubes connected
 80 to the quasi-parallel shock, mirror-mode waves, and non-reconnecting current sheets. Over-
 81 all, the knowledge of how quasi-perpendicular jets form is still very poor. While it is be-
 82 lieved that at the quasi-parallel shock rippling (Hietala et al., 2009; Hietala & Plaschke,
 83 2013) and shock reformation (Raptis et al., 2020) can lead to jet formation, it is not clear
 84 whether these or similar mechanisms can lead to jets also at the quasi-perpendicular shock,
 85 where the scales of such processes are typically much smaller.

86 Understanding how solar wind conditions affect jet formation can help us inves-
 87 tigate how they form. The IMF cone angle had long been considered as the only param-
 88 eter controlling magnetosheath occurrence (e.g., Plaschke et al., 2013). Now that even
 89 larger data sets are available, mainly thanks to Time History of Events and Macroscale
 90 Interactions during Substorms (THEMIS; Angelopoulos, 2008) and Magnetospheric Mul-
 91 tiscale Mission (MMS; Burch et al., 2016) missions' dayside configurations, this picture
 92 is becoming more complicated. Recently, LaMoury et al. (2021) studied separately the
 93 solar wind conditions affecting the formation of jets and their ability to propagate to the
 94 magnetopause by separating the data into regions close to the bow shock and close to
 95 the magnetopause. The subset close to the bow shock can be considered to be dominated
 96 by formation effects, while the near-magnetopause subset is also affected by propagation
 97 effects. They reported that, in addition to IMF cone angle, the solar wind conditions fa-
 98 vorable for jet formation are low IMF strength (B), low density (n), low dynamic pres-
 99 sure (P_{dyn}), high plasma beta (β), and high Alfvén Mach number (M_A). Koller et al.
 100 (2022) studied the occurrence of magnetosheath jets during large-scale solar wind struc-
 101 tures. They found that jet occurrence was increased by $\sim 50\%$ during stream-interaction
 102 regions and high-speed streams, but decreased by $\sim 50\%$ during coronal mass ejections'
 103 sheath regions and magnetic ejecta. This was attributed to different plasma and mag-
 104 netic field characteristics of the different large scale structures affecting jet formation.
 105 However, Vuorinen et al. (submitted) investigated THEMIS observations over solar cy-
 106 cle 24, and their results suggest that the yearly jet occurrence rates do not change strongly
 107 across a solar cycle and are dominated by cone angle effects.

108 In this paper, we study the solar wind influence on jet formation in more detail.
 109 We focus on jets that are generated at the Earth's bow shock and have a significant earth-
 110 ward velocity component. These jets may have the possibility to impact the magnetopause
 111 and consequently perturb the magnetosphere and the ionosphere. In particular, we sta-
 112 tistically investigate the two regimes, low and high IMF cone angles, separately, as they
 113 are linked to the two well-established distinct shock regimes: quasi-parallel and quasi-
 114 perpendicular, respectively. We find that low IMF cone angle jet formation is not con-
 115 trolled by other solar wind parameters, but during high IMF cone angles certain solar
 116 wind conditions (e.g., high M_A and β) are more favorable for jet formation. First, we
 117 introduce the data and methods applied in this study. Second, we present the statisti-
 118 cal results and show examples of jet observations at multiple quasi-perpendicular shock

119 crossings of different upstream β and M_A conditions. Finally, we discuss the implications
 120 and caveats followed by the conclusions of this study.

121 2 Data and Methods

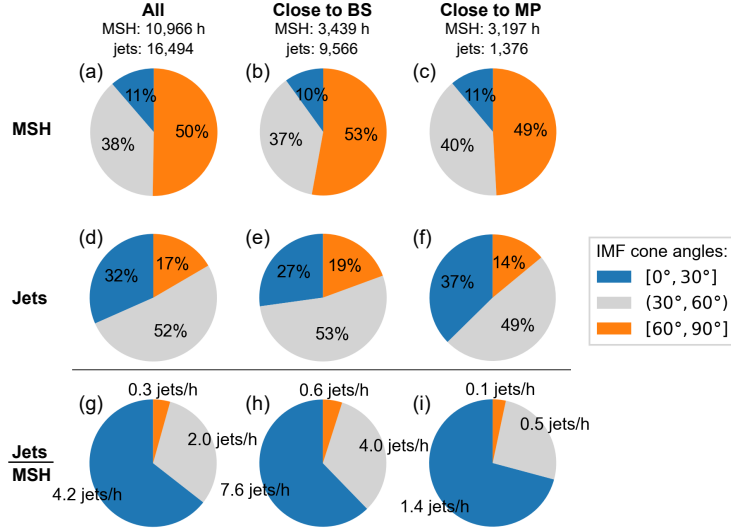


Figure 1. Percentages of the THEMIS (a–c) magnetosheath (MSH) observations and (d–f) jet observations in the three different IMF cone angle bins. Panels (g–i) show the average number of observed jets per hour of magnetosheath observations. The left-most column (a,d,g) uses all MSH and jet data, the middle column (b,e,h) includes only data close to the bow shock ($F \geq 0.5$), and the right-most column (c,f,i) only data close to the magnetopause ($F \leq 0.25$).

122 We investigate subsolar magnetosheath data from the THEMIS probes (Angelopoulos,
 123 2008) from the years 2008–2020. We use data from the Fluxgate Magnetometer (FGM;
 124 Auster et al., 2008) and the Electrostatic Analyzer (ESA; McFadden et al., 2008). The
 125 statistical data set uses on-board moment data and all observations have been interpo-
 126 lated to a common 1-s cadence. This is a relevant step to note when considering jet du-
 127 rations and comparisons with other missions. This particular THEMIS magnetosheath
 128 and jet data set has been created using the algorithm presented by Plaschke et al. (2013)
 129 (see their paper for details) and was first used by Koller et al. (2022). It is publicly avail-
 130 able (Koller et al., 2021). At the end of this paper, we present a few examples of shock
 131 crossings. In these examples, we use THEMIS ground data (available during fast sur-
 132 vey mode intervals). We also look at Magnetospheric Multiscale Mission (MMS) space-
 133 craft data of two different bow shock crossings. We use fluxgate magnetometer (Russell
 134 et al., 2016) data and burst-resolution Fast Plasma Instrument (FPI; Pollock et al., 2016)
 135 ion data. The high cadence of MMS observations allows us to investigate the shock cross-
 136 ings in significantly better temporal detail than THEMIS.

137 The main jet criterion is that at some point in a magnetosheath jet, the earthward
 138 dynamic pressure has to exceed half of the solar wind dynamic pressure. The jet inter-
 139 val is defined as the period when the earthward dynamic pressure in the magnetosheath
 140 is larger than one quarter of the solar wind dynamic pressure. Within 1-minute inter-
 141 vals around the jet interval, V_X (in GSE coordinates) in the magnetosheath has to ex-
 142 ceed $V_X(t_0)/2$ (t_0 is the time when the dynamic pressure ratio reaches its peak within
 143 the jet). This ensures that jets exhibit an increase in earthward flow speed. Note that
 144 this criterion means that not every enhancement of dynamic pressure is considered a jet.

145 The measurements at t_0 of each jet represent the jet observations in our statistical study.
 146 The solar wind conditions for each of the magnetosheath (and jet) measurements are ob-
 147 tained from the OMNI high-resolution 1-min data set (King & Papitashvili, 2005). How-
 148 ever, we apply a running average of the five preceding minutes to obtain a more reliable
 149 estimate of the general solar wind conditions at the time of jet formation.

150 As demonstrated by LaMoury et al. (2021), it is important to disentangle solar wind
 151 influence on jet formation and jet propagation. Thus, we only use data from the outer-
 152 most half of the magnetosheath close to the bow shock. We select the data by assign-
 153 ing each THEMIS observation a relative radial position F in the magnetosheath (mag-
 154 netopause at $F = 0$ and bow shock at $F = 1$)

$$F = (r - r_{\text{MP}})/(r_{\text{BS}} - r_{\text{MP}}) \quad (1)$$

155 by applying Shue et al. (1998) magnetopause model and Merka et al. (2005) bow shock
 156 model. Here r is the geocentric distance of the spacecraft. r_{BS} and r_{MP} are the geo-
 157 centric distances of the model bow shock and magnetopause, respectively, measured along
 158 the line connecting the spacecraft and the center of the Earth. We use the constraint $F \in$
 159 $[0.5, 1.1]$, because we want to maximize the number of observations to obtain the best
 160 possible statistics. The jet occurrence has not decreased significantly before half-way ($F =$
 161 0.5) through the magnetosheath (not shown here, but can be seen in Figure 1 of LaM-
 162 oury et al., 2021), implying that propagation effects are not yet significant. There are
 163 uncertainties both in the bow shock and magnetopause models and in the OMNI data,
 164 which is why we accept values up to $F = 1.1$, where the jet occurrence quickly decreases.

165 In order to study the quasi-parallel and quasi-perpendicular regimes separately, we
 166 divide the observations by the IMF cone angle

$$\alpha = \arccos(|B_X|/B) \in [0^\circ, 90^\circ], \quad (2)$$

167 where B_X is the X component of the magnetic field vector in GSE coordinates. The cone
 168 angle distributions of jet and magnetosheath (MSH) observations of the data set are shown
 169 in Figure 1 for the whole data set and also separately for observations close to the model
 170 bow shock and close to the model magnetopause. Quasi-parallel (quasi-perpendicular)
 171 regime is represented by low (high) cone angles $\leq 30^\circ$ ($\geq 60^\circ$). Vuorinen et al. (2019)
 172 showed that for these extreme ranges of cone angles, the jet occurrence rates are spa-
 173 tially uniform in the subsolar region. For the intermediate values ($30^\circ, 60^\circ$), one part of
 174 the subsolar magnetosheath is downstream of the quasi-parallel and the other downstream
 175 of the quasi-perpendicular shock, and thus the jet occurrence rate varies spatially. To
 176 clearly separate these two regimes, we exclude the data with such intermediate cone an-
 177 gles. Figure 1 displays that close to the bow shock, where we are focusing on in this study,
 178 27% of jets in the THEMIS data occurred during low IMF cone angles and 19% occurred
 179 during high IMF cone angles. In contrast, only 10% of MSH observations were taken
 180 during low IMF cone angle conditions and 53% during high IMF cone angles. This il-
 181 lustrates that jets are much more common during low IMF cone angles, but as high IMF
 182 cone angle conditions are more frequent at Earth, quasi-perpendicular jets make up a
 183 significant portion of jets in the Earth's magnetosheath.

184 We apply Bayes' theorem

$$P(\text{jet}|\text{conditions}) = \frac{P(\text{conditions}|\text{jet})P(\text{jet})}{P(\text{conditions})} \quad (3)$$

185 to calculate conditional probabilities, i.e., normalized jet occurrence rates under differ-
 186 ent solar wind conditions. The probabilities on the right-hand side of the equation can
 187 be estimated using the observations: $P(\text{jet}) = N_{\text{jet}}/N_{\text{msh}}$, $P(\text{conditions}) = N_{\text{msh}}(\text{conditions})/N_{\text{msh}}$,
 188 and $P(\text{conditions}|\text{jet}) = N_{\text{jet}}(\text{conditions})/N_{\text{jet}}$. Thus, the equation becomes

$$P(\text{jet}|\text{conditions}) = \frac{N_{\text{jet}}(\text{conditions})}{N_{\text{msh}}(\text{conditions})}. \quad (4)$$

189 Because jets are mostly observed during smaller cone angles but higher cone angles are
 190 more frequent in the whole magnetosheath data set, without the separation by IMF cone
 191 angles we would be generally comparing jets and magnetosheath observations during very
 192 different IMF cone angle conditions. Low and high IMF cone angle solar wind have sta-
 193 tistically different distributions in other parameters (not shown here). This means that
 194 without taking the IMF cone angle into account in the normalization, the normalized
 195 occurrence rates can just reflect the differences between low and high IMF cone angle
 196 solar wind conditions. In high-dimensional data sets, it can be difficult to account for
 197 all the interdependencies of different parameters. However, classifying the data with the
 198 IMF cone angle is important and meaningful as there are very strong differences in IMF
 199 cone angle distributions between jet and MSH data sets, and quasi-parallel and quasi-
 200 perpendicular shock regimes are well-established and known to be different.

3 Results

3.1 THEMIS Statistical Results

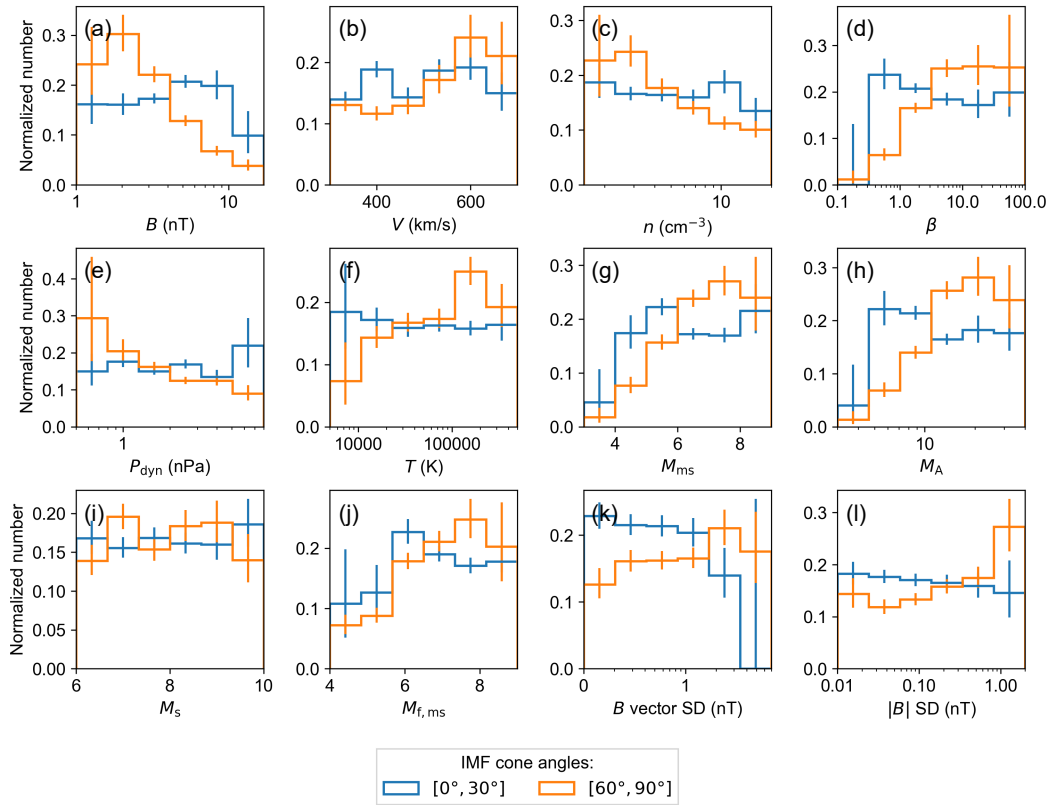


Figure 2. Distributions showing the normalized occurrence rates of jets (jets distribution normalized by the magnetosheath distribution) as functions of OMNI IMF and solar wind parameters: (a) IMF magnitude, (b) speed, (c) density, (d) β , (e) dynamic pressure, (f) ion temperature, (g) magnetosonic Mach number, (h) Alfvén Mach number, (i) sonic Mach number, (j) fast magnetosonic Mach number, (k) IMF vector standard deviation, and (l) IMF magnitude standard deviation. The distributions are shown separately for observations during low ($[0^\circ, 30^\circ]$; blue) and high IMF cone angles ($[60^\circ, 90^\circ]$; orange). The error bars denote 95 % proportional confidence intervals.

203 In Figure 2, we present the normalized distributions of jet occurrence as a func-
 204 tion of the OMNI solar wind parameters. The blue histograms represent low IMF cone
 205 angles ($\leq 30^\circ$) and the orange histograms represent high IMF cone angles ($\geq 60^\circ$). There
 206 seems to be a threshold for jet formation, as it is effectively suppressed for very low $\beta \lesssim$
 207 0.5 and $M_A \lesssim 5$ conditions for both quasi-parallel and quasi-perpendicular regimes. How-
 208 ever, during low IMF cone angle conditions, there are only 2–3 h of magnetosheath data
 209 in these low β and M_A bins. Overall, we can see that for low IMF cone angles (down-
 210 stream of the quasi-parallel shock), the distributions are relatively flat (within error bars),
 211 while there are clear trends in many distributions for high IMF cone angles. A flat his-
 212 togram indicates that the parameter has no influence on jet formation, as we see no pref-
 213 erence in the data for any particular values. However, trends in the histograms indicate
 214 that there is a preference, i.e., jets are more often observed during certain solar wind con-
 215 ditions. The results indicate that conditions favorable for jet formation during high IMF
 216 cone angles (downstream of the quasi-perpendicular shock) are especially: low B , low
 217 n , high β , and high Mach numbers (except for sonic Mach number). Also low P_{dyn} , high
 218 V , and high T seem to be favorable for quasi-perpendicular jet occurrence. Although not
 219 shown here, similar results for solar wind conditions are obtained when looking at short-
 220 and long-duration jets separately.

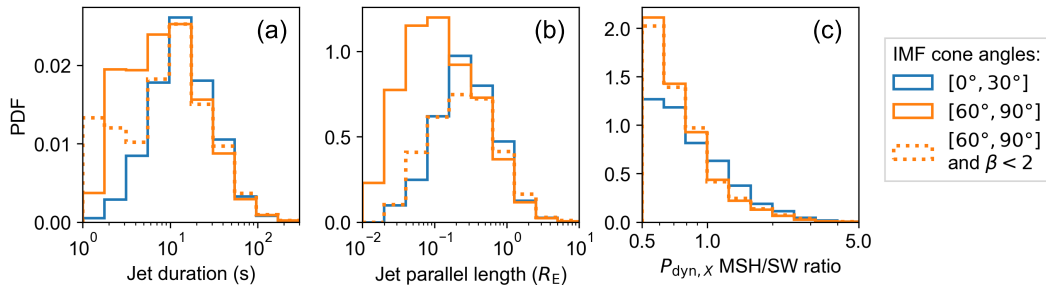


Figure 3. Distributions of (a) jet duration, (b) jet length parallel to $\mathbf{v}(t_0)$, and (c) $P_{\text{dyn},x}$ ratio between the magnetosheath value and the solar wind value at t_0 . The distributions are shown separately for low IMF cone angles (solid blue), high IMF cone angles (solid orange), and high IMF cone angles with SW $\beta < 2$ (dotted orange).

221 In Figure 3, we show the distributions of jet durations, lengths parallel to the jet
 222 propagation direction $\mathbf{v}(t_0)$, and the ratio of jet and solar wind earthward dynamic pres-
 223 sure for low (blue solid line) and high (orange solid line) IMF cone angles separately. Dur-
 224 ing high IMF cone angles, the jets tend to be clearly smaller (both in duration and par-
 225 allel length; Figures 3a&b). The quasi-perpendicular jet size distribution peaks at $\sim 0.1 R_E$.
 226 Small jets are much less common during low IMF cone angles, and the size distribution
 227 of quasi-parallel jets peaks at ~ 15 s and $\sim 0.3 R_E$. Jets are also weaker during high
 228 IMF cone angles as can be seen in Figure 3c. We have additionally included the histograms
 229 representing jets observed during high IMF cone angle and $\beta < 2$ conditions. We can
 230 see that for parallel lengths, this histogram is more similar to the distribution of jets dur-
 231 ing low IMF cone angles. This shows that for high IMF cone angle conditions or the quasi-
 232 perpendicular shock, high $\beta > 2$ (or high M_A , although not shown here) in particular
 233 increases the formation of small jets. This does not account for the whole difference in
 234 jet occurrence rates for low and high β , as jets of all sizes are more common during high
 235 β . There is no such difference in the distributions of jet strengths (MSH/SW dynamic
 236 pressure ratios) between low and high β conditions.

237
238

3.2 Examples of Quasi-Perpendicular Bow Shock Crossings During Different β and M_A Conditions

239
240
241
242
243
244
245
246
247

To better understand the statistical results for jets during high IMF cone angles, we present examples of quasi-perpendicular shock crossings observed by THEMIS and MMS during different solar wind β and M_A conditions. We show four events, which show us how the structure of the shock changes with increasing β and M_A , and how that relates to observations of downstream jets. We move from low to high β and M_A . We use the Plaschke et al. (2013) jet algorithm to look for jets in the data. Two of the events (Event 2 and Event 3) are THEMIS multi-spacecraft events, in which we can confirm the quasi-perpendicular geometry and β and M_A conditions with simultaneous local upstream measurements instead of relying only on OMNI measurements.

248
249
250
251
252
253
254
255
256
257
258
259
260
261
262
263
264
265
266
267
268
269
270
271

Figure 4 shows Event 1: MMS1 was crossing from the solar wind to the magnetosheath on March 4, 2019, around $\sim 22:42$ UT. MMS1 was located at $[15.4, -3.2, 1.8] R_E$ (in GSE). Both OMNI and local measurements in the solar wind show a quasi-perpendicular geometry. The ion spectrogram also shows a lack of > 10 keV ions consistent with this. We estimate $\theta_{Bn} = 65^\circ$ for OMNI and 71° for local upstream measurements, respectively, using Merka et al. (2005) bow shock model. Local measurements from the upstream region 22:41–22:42 yield solar wind $\beta = 1.7$ and $M_A = 5.7$, which are in relatively close agreement with OMNI ($\beta = 0.65$ and $M_A = 6.0$). These represent low β and M_A conditions for jets (see Figure 2 statistics). We note that density and temperature observations of MMS FPI instrument can be unreliable in the solar wind due to the narrowness of the solar wind beam, and thus there is uncertainty especially in β . The left panel of Figure 4 shows an overview of the with data resampled to 0.5 s cadence. We see a relatively abrupt quasi-perpendicular shock crossing with foot, overshoot, and undershoot signatures. The downstream region of the shock exhibits little structure, and the Plaschke et al. (2013) algorithm finds one small and weak jet (highlighted in magenta) for this data. The right panel of Figure 4 is a zoom-in into the magnetosheath. For direct comparison with the statistical THEMIS data set, we show the measurements downsampled to 3 s and then interpolated to 1 s (thick lines). The instrument data rate measurements (FGM: 62.5 ms, FPI: 150 ms) are shown in thin lines. The Plaschke et al. (2013) algorithm finds two very small jets when applied on instrument burst level data, but no detection when using the data downsampled to 3 s and interpolated to 1 s. Note that in this event, the OMNI dynamic pressure is lower than the local upstream dynamic pressure, which means that these jets would likely not be identified if we used the local measurements for the threshold.

272
273
274
275
276
277
278
279
280
281
282
283
284
285

Next, we look at Event 2 observations by THEMIS A, D, and E spacecraft on May 11, 2015, around $\sim 21:00$ UT. The spacecraft were all located near the bow shock nose. These locations are shown in Figure 5. THEMIS A was in the solar wind, THEMIS E crossed the bow shock from the magnetosheath to the solar wind, and THEMIS D was in the magnetosheath (see Figure 6). Figure 5 also shows a model bow shock shape (Merka et al., 2005) and the estimated bow shock normal at the point closest to THEMIS E. We have plotted the average magnetic field vectors during 20:57–21:02 UT measured by OMNI and by THEMIS A in the solar wind. We see that the bow shock was clearly very perpendicular: $\theta_{Bn} = 84^\circ$ based on THEMIS A observations and $\theta_{Bn} = 89^\circ$ based on OMNI observations. The solar wind β and M_A were, respectively, 5.5 and 16 according to OMNI and 2.4 and 8.5 according to local THEMIS A observations in the upstream. We note that temperature observations of THEMIS ESA instrument can be unreliable in the solar wind due to the narrowness of the solar wind beam, and thus there is uncertainty especially in β .

286
287
288
289

Figure 6 shows the measurements from these three locations. THEMIS A observes no foreshock and quite steady solar wind. Nearby THEMIS E crosses from the magnetosheath into the solar wind with a shock transition region in between. This transition region is structured with more variations in magnetic field, density, and velocity com-

pared the magnetosheath proper that was observed before. Two 15–20 s and three smaller jets can be identified within this transition region. THEMIS D further in the magnetosheath observes the much less structured and higher temperature magnetosheath proper. Figure 7 is a zoom-in of THEMIS E observations during the quasi-perpendicular transition region. Here the data are interpolated to 1 s cadence to be comparable with the statistical data set. Note that changing the cadence of the data changes the lengths of the jet intervals. The first two jets exhibit significant increases in earthward flow velocity, while the other jets are driven by density increases. The first jet is a strong one in terms of its earthward dynamic pressure ratio ($\sim 90\%$) while the others are weak.

Next, let us look at Event 3 observations by THEMIS B and C on August 10, 2009, around $\sim 20:10$ UT. Figure 8 shows the positions of the spacecraft, and the observed magnetic field orientations by OMNI and THEMIS C in the solar wind at 20:10–20:15. Figure 9 shows the observations of THEMIS C in the upstream and THEMIS B crossing the bow shock from the magnetosheath to the solar wind. The solar wind β and M_A were, respectively, 170 and 93 according to OMNI and 100 and 55 according to local THEMIS C observations in the upstream. The IMF magnitude is remarkably low in this event, as THEMIS C is observing $B \sim 1$ nT. Because the M_A is so extremely high, the Merka et al. (2005) bow shock model does not produce realistic bow shock shape anymore (in Figure 8 we have plotted a model bow shock shape with a higher magnetic field magnitude $B = 2$ nT for illustration). However, we can estimate θ_{Bn} with the IMF cone angle. OMNI measurements yield an IMF cone angle of 86° and the local THEMIS C observations yield the same value. As the THEMIS B and C spacecraft are observing the subsolar region, θ_{Bn} has to be very high with this perpendicular field. The lack of > 10 keV ions in the ion energy spectrogram is again consistent with this.

While THEMIS C observes relatively steady upstream conditions, THEMIS B crossing the bow shock observes a prolonged transition of magnetosheath plasma to the solar wind plasma (Figure 9). This shock crossing exhibits a train of high-amplitude magnetic field enhancements in the upstream region, which grow larger towards the shock. Note the arrow on the top of the THEMIS B panel, which indicates the beginning of the magnetosheath interval in which we search for jets. One very short-duration jet and two ~ 20 s jets can be identified within this interval with the ground reduced ESA data. Figure 10 is a zoom-in to THEMIS B observations downstream during 20:09:20–21:15:20 UT. In this interval, right downstream of the shock, the flow velocity has already decreased substantially and the density has increased, but there are still high-amplitude variations in magnetic field and density. The second jet exhibits a high increase in earthward velocity. Before this zoom-in window, THEMIS B observes magnetosheath with less variations and higher temperature (see Figure 9). We again interpret this as the shock having a structured transition layer, which also contains jets, and deeper in the magnetosheath these variations have dissipated.

In Figure 11, we present Event 4: MMS1 burst observations of another very high $\beta \sim 70$ and $M_A \sim 60$ quasi-perpendicular bow shock crossing on November 25, 2017, around $\sim 23:40$ UT. This event serves as an extreme example of how the quasi-perpendicular magnetosheath can exhibit a high degree of structuring during high solar wind β and M_A , and how it is resolved by high-resolution MMS measurements. The data in the left panel (with the exception of the ion spectrogram) have been downsampled to 2-s cadence. This bow shock crossing and its upstream structure has been studied in detail by Petrukovich and Chugunova (2021), but they did not focus on the magnetosheath downstream of the shock. Petrukovich and Chugunova (2021) calculated the θ_{Bn} to be 68° based on OMNI observations and 59° based on local measurements in the upstream region, yielding a quasi-perpendicular geometry. We can see a periodic train of high-amplitude magnetic field and density enhancements in the upstream region and at the extended shock crossing. Petrukovich and Chugunova (2021) placed the shock crossing at 23:38 UT, when the mag-

342 netosheath flow becomes more steady. MMS1 GSE position was [12.8, 5.7, 2.4] R_E at this
 343 point in time.

344 The fluctuations are also present in the downstream. Their period is ~ 20 s. How-
 345 ever, no jets can be identified in this data as the variations in V_X component are too low
 346 in these timescales. Note that we only execute the search when there are OMNI solar
 347 wind dynamic pressure observations available for the preceding minute, here within 23:27–
 348 23:33 UT. The right-hand panel shows a zoom-in to the magnetosheath. Here the thicker
 349 lines represent data first downsampled to a 3-s resolution and then interpolated to a 1-
 350 s cadence, to be directly comparable with the data used to construct the THEMIS jet
 351 data set. Again, no jets are found using this data. The thinner lines represent the data
 352 at instrument resolutions (FGM: 62.5 ms, FPI: 150 ms). The jet detection algorithm iden-
 353 tifies many of these density enhancements as jets in the burst-resolution plasma data.
 354 This is due to short timescale (a few seconds) variations in V_X , which allow them to ful-
 355 fill the Plaschke et al. (2013) criteria. Again, deeper in the magnetosheath (before the
 356 zoomed-in window), the level of fluctuations is much lower and jets are not identified.

357 4 Discussion

358 On top of the now well-established link between jets and low IMF cone angles, or
 359 the quasi-parallel shock, LaMoury et al. (2021) found additional parameters affecting jet
 360 formation. They concluded that low B , low n , high β , and high M_A are favorable con-
 361 ditions for jet generation. According to our detailed study, these results apply to jets form-
 362 ing during high IMF cone angle conditions. During low IMF cone angles, other solar wind
 363 parameters do not have a significant influence on jet occurrence. However, jet occurrence
 364 is very effectively suppressed for very low $\beta \lesssim 0.5$ and $M_A \lesssim 5$ conditions for both
 365 quasi-parallel and quasi-perpendicular regimes (although there is statistical uncertainty
 366 for the quasi-parallel case). This corresponds relatively well with the threshold ($M_A \sim$
 367 2–3) where the shock becomes subcritical and ceases to reflect particles (Burgess et al.,
 368 2012; Kennel et al., 1985). In other words, substantial ion reflection seems to be a key
 369 ingredient for jet formation. Tinoco-Arenas et al. (2022) studied 2D local hybrid sim-
 370 ulations of shocks with parameters close to these threshold values. They used $\beta = 0.5$
 371 and varied θ_{Bn} and M_A . They found jets within the whole parameter range $M_A \in [4.28, 7.42]$.

372 Separating the data to low and high IMF cone angles is important as most jets are
 373 observed during lower IMF cone angles and most magnetosheath measurements are made
 374 during higher cone angles. Thus, when normalizing the jet data by the magnetosheath
 375 data (i.e., calculating conditional probabilities; Eq. 4) without this distinction (as in LaM-
 376 oury et al., 2021), the results will be exhibiting differences in solar wind characteristics
 377 during low and high IMF cone angles rather than only in jet occurrence rates. Classi-
 378 fying the data by cone angles removes this effect and allows us to better compare the
 379 occurrence rates during different solar wind conditions. Goncharov et al. (2020) also stud-
 380 ied jets in the quasi-parallel and quasi-perpendicular dayside magnetosheath, including
 381 flank observations, with slightly different jet criteria and a smaller MMS data set. They
 382 did not normalize for relative radial position in the magnetosheath, i.e., separate forma-
 383 tion and propagation. They also did not separate the normalizing magnetosheath data
 384 into these two regimes, which we argue is important because otherwise we end up com-
 385 paring lower IMF cone angle jet observations mostly to higher IMF cone angle magne-
 386 tosheath observations. Their results suggested that jets are more common during higher
 387 magnetic field magnitude, solar wind speed, M_A , and β . The last two results are in agree-
 388 ment with our results (but only for the quasi-perpendicular case), but the first two are
 389 not. The favorability they observed for higher solar wind speed may be explained by their
 390 criterion for higher dynamic pressure jets and by propagation effects (LaMoury et al.,
 391 2021). Similarly, high magnetic field magnitude is favorable for jet propagation deep into
 392 the magnetosheath.

393 We also statistically studied the durations of jets, their lengths parallel to their prop-
 394 agation direction, and their dynamic pressure ratios (i.e., strengths). We find that the
 395 durations of quasi-parallel jets peak at a little more than 10 s duration. This is compa-
 396 rable to the period of ULF waves in the terrestrial ion foreshock. According to our re-
 397 sults, quasi-perpendicular jets tend to be smaller than quasi-parallel ones, which agrees
 398 with previous studies (e.g., Raptis et al., 2020; Goncharov et al., 2020). We also find that
 399 quasi-perpendicular jets tend to have a lower $P_{\text{dyn},X}$ MSH/SW ratio, meaning that they
 400 are weaker, as also found by Raptis et al. (2020). When taking a low plasma beta sub-
 401 set ($\beta < 2$) of the high IMF cone angle set, we find that they seem to be more simi-
 402 lar to low IMF cone angle jets in their size distribution. The high beta quasi-perpendicular
 403 subset ($\beta \geq 2$) represents the newly resolved population of the smallest jets. However,
 404 jets of all sizes are more common during high β .

405 While OMNI data allow us to link every magnetosheath observation to a solar wind
 406 measurement, this data set is known to contain uncertainty (e.g., Walsh et al., 2019; Vokhmyanin
 407 et al., 2019). OMNI data are combined from multiple spacecraft at L1 and then propa-
 408 gated to the Earth’s bow shock. While this data are very useful for large statistical stud-
 409 ies where errors can be assumed to average out, one cannot blindly trust it when look-
 410 ing at individual events. Because quasi-perpendicular jets have significantly lower oc-
 411 currence rate than quasi-parallel jets, a number of the high IMF cone angle jets in this
 412 data set have certainly been misclassified, and in reality they have formed at the quasi-
 413 parallel shock. For individual events, it is important to use local upstream measurements
 414 to verify the shock geometry. Similarly, the bow shock model (Merka et al., 2005) and
 415 the magnetopause (Shue et al., 1998) model contain uncertainty. We note the models
 416 have ranges of solar wind values where they are valid, and thus the leftmost and right-
 417 most bins in Figure 2 are most unreliable in terms of F values. The assumption that data
 418 with $F \in [0.5, 1.1]$ are close to the bow shock may therefore not strongly hold in these
 419 bins.

420 We provided four examples of multi-spacecraft quasi-perpendicular shock crossings
 421 with varying β and M_A to give context on how the quasi-perpendicular shock transition
 422 changes with increasing β and M_A and how these dynamics may be linked to jet forma-
 423 tion. We used local upstream observations including simultaneous two-point measure-
 424 ments by THEMIS to verify the steady quasi-perpendicular geometry and the high β and
 425 M_A in the solar wind. With increasing β and M_A the shock transition becomes more
 426 extended. Note, however, that the observed duration depends on the relative motion be-
 427 tween the shock and the spacecraft. The so-called transition region exhibits high-amplitude
 428 variations particularly in magnetic field magnitude and density. There is no clear anti-
 429 correlation between magnetic field magnitude and density, so we do not consider these
 430 mirror mode waves, which are typical in the quasi-perpendicular magnetosheath proper.
 431 In contrast, the magnetic field and density are often enhanced together. There are also
 432 enhancements of dynamic pressure and some of these can be identified as earthward jets
 433 by the Plaschke et al. (2013) criterion. These jets are indeed present in the shock tran-
 434 sition region but were not recorded in our examples deeper in the magnetosheath. A sta-
 435 tistical investigation also revealed that quasi-perpendicular jets during high M_A solar
 436 wind conditions typically occur very close to the model bow shock (not shown). Thus,
 437 these type of jets are probably not very likely to go on and impact the magnetopause,
 438 perhaps as they dissipate in the transition region.

439 Previous observations of the Earth’s quasi-perpendicular bow shock during high
 440 M_A (Sundberg et al., 2017; Madanian et al., 2021) and high β (Petrukovich & Chugunova,
 441 2021) (high M_A and high β are tied to each other at Earth’s heliocentric distance) show
 442 that such shock crossings are extended and exhibit high magnitude structures both up-
 443 stream and downstream. These structures form upstream due to reflected ion dynam-
 444 ics, which become important for dissipating energy in these conditions. Sundberg et al.
 445 (2017) presented Cluster observations from three quasi-perpendicular shock crossings,

446 and suggested that the observed non-stationarities of the shock could be due to the ion
 447 Weibel instability. Petrukovich and Chugunova (2021) concluded that the observed struc-
 448 tures are not mirror mode waves typically observed in the quasi-perpendicular magne-
 449 tosheath. They claimed that they are most likely due to shock reformation, although they
 450 did not provide any direct evidence. Madanian et al. (2021) named these upstream struc-
 451 tures “proto-shocks”, which are a part of quasi-periodic shock reformation. They con-
 452 cluded that these structures are created by the reflected ions at the edge of the foot, and
 453 then they grow non-linearly while they convect towards the shock. These proto-shocks
 454 slow down the incoming solar wind and influence the reflection of particles from the shock
 455 (this is also seemingly happening in our Events 3 and 4, although not shown here). All
 456 these studies suggest that while such reformation structures are present, the main shock
 457 layer never disappears. Sulaiman et al. (2015) studied several high M_A Saturn’s bow shock
 458 crossings and showed that there is a reformation cycle typically at a period of $\sim 26\%$
 459 of the ion gyroperiod. Sundberg et al. (2017), Madanian et al. (2021), and Petrukovich
 460 and Chugunova (2021) found similar reformation structures with periods close to this
 461 value. This also fits well with the timescales of upstream structures seen in Events 3 and
 462 4 shown in our study. While typically the quasi-perpendicular shock reformation length
 463 and time scales are small in comparison to scales commonly associated with magnetosheath
 464 jets, this period can become of the order of tens of seconds when the IMF magnitude be-
 465 comes very low ($\lesssim 1$ nT).

466 The quasi-perpendicular shock can also exhibit ripples that move along the shock
 467 surface (e.g., Lowe & Burgess, 2003; Johlander et al., 2016; Madanian et al., 2021). Lowe
 468 and Burgess (2003) found their frequencies to be around a couple times the upstream
 469 ion gyrofrequency in their 2D hybrid simulations. Johlander et al. (2016) studied rip-
 470 ples at a shock crossing observed by MMS and found the ripple frequency to be three
 471 times the upstream ion gyrofrequency. Timescales of both the reformation cycle and rip-
 472 ples are dependent on the upstream ion gyrofrequency, and therefore these timescales
 473 increase for lower upstream magnetic field magnitude (for higher β and M_A conditions).
 474 This fits well with our statistical results that jets downstream of the quasi-perpendicular
 475 shock (or during high IMF cone angles) are significantly more common when the IMF
 476 magnitude is low (and β and M_A are high). This indicates that the quasi-perpendicular
 477 shock dynamics amplified and temporally/spatially enlarged by high β and high M_A up-
 478 stream conditions can also lead to the formation of jets as a by-product. As quasi-parallel
 479 jet formation has been suggested to be related to bow shock rippling (Hietala et al., 2009;
 480 Hietala & Plaschke, 2013) and Raptis et al. (2022) showed that quasi-parallel shock re-
 481 formation can lead to downstream jets, already known, or similar, mechanisms could pos-
 482 sibly explain jet formation at quasi-perpendicular shocks, as well.

483 Recently, Omidi et al. (2021) studied the spatial and temporal structure of a high
 484 M_A quasi-perpendicular shock with a global 2.5D simulation. Their simulation results
 485 indicate that upstream structures, such as previously reported for these type of shocks,
 486 can emerge in spacecraft data due to a surface wave moving along a shock and the shock
 487 crossing the spacecraft numerous times. These results highlight an important and inher-
 488 ent issue of disentangling temporal and spatial variations when analyzing single-spacecraft
 489 data. More detailed multi-spacecraft studies are needed to discard possible misclassifi-
 490 cations of bow shock crossings as jets and to study how jets move with respect to the
 491 surrounding plasma. This would help us understand their nature and formation: whether
 492 they are related to ripples moving along the shock and/or whether they are related to
 493 the processing of the solar wind at the structures of the reformation cycle and whether
 494 they can propagate far from the shock towards the magnetopause. We attempted to per-
 495 form an MMS timing analysis for the dynamic pressure fluctuations of Event 4, but the
 496 shorter-scale fluctuations made it impossible for us to cross-correlate the signals accu-
 497 rately. We note that the width of the shock transition region, and also the jets within,
 498 is dependent on the speed of the spacecraft moving in space and/or on the speed of the
 499 shock as it moves across the spacecraft.

500 Finally, we have highlighted that the time resolution of observations can have an
 501 effect on whether a jet algorithm classifies a certain structure as a jet. Thus, different
 502 data sets may yield relatively more or fewer jets due to differences in cadences. This is
 503 important to consider when comparing or combining data from different instruments and
 504 missions.

505 5 Conclusions and Summary

506 In this study, we have statistically studied how solar wind conditions influence jet
 507 occurrence in the two regimes of low and high IMF conditions using an extensive THEMIS
 508 spacecraft data set from the years 2008–2020. This allows us to better understand jet
 509 formation at the quasi-parallel and quasi-perpendicular shocks, respectively. Jet forma-
 510 tion is observed to commence for $\beta \gtrsim 0.5$ and $M_A \gtrsim 5$ for both shock geometries. We
 511 found that during low IMF cone angles, jet occurrence close to the bow shock is not sen-
 512 sitive to the other solar wind parameters. In contrast, during high IMF cone angle con-
 513 ditions, jet formation changes as a function of other solar wind parameters: quasi-perpendicular
 514 jets are more frequently observed when the IMF magnitude is low, the SW speed is high,
 515 the SW density is low, the plasma beta is high, and the Alfvén Mach number is high.
 516 The quasi-parallel jets have an intrinsic scale size: the distribution of sizes (parallel to
 517 flow) peaks at ~ 15 s and $\sim 0.3 R_E$. The jets formed during high IMF cone angles (or
 518 at the quasi-perpendicular shock) are smaller in size and weaker in dynamic pressure than
 519 those observed during low IMF cone angles. In particular, these small jets tend to form
 520 during high β and M_A conditions.

521 We presented examples of quasi-perpendicular shock crossings during different so-
 522 lar wind β and M_A conditions, illustrating that when these parameters increase, the shock
 523 dynamics change and the shock transition becomes more extended in agreement with
 524 previous studies. In particular, we showed the shock transition region exhibits large-amplitude
 525 variations not only in the magnetic field and density, but also in dynamic pressure. Earth-
 526 ward magnetosheath jets were consequently found in this transition region. They may
 527 be related to the reformation of the quasi-perpendicular shock, as the reformation and
 528 rippling time scales become larger for decreasing magnetic field magnitude (or increas-
 529 ing β and M_A). Deeper in the magnetosheath the plasma structuring has dissipated and
 530 at least in these particular events we did not see jets there. This indicates that these types
 531 of quasi-perpendicular jets are not expected to be geoeffective. However, they are a part
 532 of high β and high M_A shock dynamics, and their relevance may be more significant at
 533 shock environments where the magnetic field obliquity, β , and M_A are frequently higher.
 534 We note that future multi-spacecraft studies are needed to clarify how these jets prop-
 535 agate, and consequently to confirm that they are not simply signatures of the shock mov-
 536 ing across the spacecraft due to surface waves.

537 Open Research

538 THEMIS and OMNI data can be accessed via, e.g., NASA’s Coordinated Data Anal-
 539 ysis Web (<https://cdaweb.gsfc.nasa.gov/>). The magnetosheath and jet data set used in
 540 this study can be found at Koller et al. (2021).

541 Acknowledgments

542 LV acknowledges the financial support of the University of Turku Graduate School. HH
 543 and ATL were supported by Royal Society awards URF\R1\180671 and RGF\EA\181090.
 544 HH thanks for support by the International Space Science Institute (ISSI) in Bern, through
 545 ISSI International Team project #465 ”Foreshocks Across The Heliosphere: System Spe-
 546 cific Or Universal Physical Processes?”. FP is supported by the German Ministerium
 547 für Wirtschaft und Klimaschutz and the German Zentrum für Luft- und Raumfahrt un-

548 der contract 50 OC 2201. We acknowledge NASA contract NAS5-02099 and V. Angelopou-
 549 los for use of data from the THEMIS Mission.

550 References

- 551 Angelopoulos, V. (2008). The THEMIS Mission. *Space Science Reviews*, *141*(1), 5.
 552 doi: 10.1007/s11214-008-9336-1
- 553 Archer, M. O., & Horbury, T. S. (2013). Magnetosheath dynamic pressure enhance-
 554 ments: occurrence and typical properties. *Annales Geophysicae*, *31*(2), 319–
 555 331. doi: 10.5194/angeo-31-319-2013
- 556 Archer, M. O., Horbury, T. S., & Eastwood, J. P. (2012). Magnetosheath pressure
 557 pulses: Generation downstream of the bow shock from solar wind disconti-
 558 nities. *Journal of Geophysical Research*, *117*(December 2011), 1–13. doi:
 559 10.1029/2011JA017468
- 560 Auster, H. U., Glassmeier, K. H., Magnes, W., Aydogar, O., Baumjohann, W.,
 561 Constantinescu, D., ... Wiedemann, M. (2008). The THEMIS Flux-
 562 gate Magnetometer. *Space Science Reviews*, *141*(1-4), 235–264. doi:
 563 10.1007/s11214-008-9365-9
- 564 Burch, J. L., Moore, T. E., Torbert, R. B., & Giles, B. L. (2016). Magnetospheric
 565 Multiscale Overview and Science Objectives. *Space Science Reviews*, *199*(1), 5-
 566 21. doi: 10.1007/s11214-015-0164-9
- 567 Burgess, D., Möbius, E., & Scholer, M. (2012). Ion Acceleration at the Earth’s Bow
 568 Shock. *Space Science Reviews*, *173*(1), 5-47. doi: 10.1007/s11214-012-9901-5
- 569 Goncharov, O., Gunell, H., Hamrin, M., & Chong, S. (2020). Evolution of high-
 570 speed jets and plasmoids downstream of the quasi-perpendicular bow shock.
 571 *Journal of Geophysical Research: Space Physics*, *125*(6), e2019JA027667.
 572 (e2019JA027667 2019JA027667) doi: <https://doi.org/10.1029/2019JA027667>
- 573 Hietala, H., Laitinen, T. V., Andréevová, K., Vainio, R., Vaivads, A., Palmroth,
 574 M., ... Rème, H. (2009). Supermagnetosonic Jets behind a Collision-
 575 less Quasiparallel Shock. *Physical Review Letters*, *103*(24), 245001. doi:
 576 10.1103/PhysRevLett.103.245001
- 577 Hietala, H., & Plaschke, F. (2013). On the generation of magnetosheath high-speed
 578 jets by bow shock ripples. *Journal of Geophysical Research: Space Physics*,
 579 *118*(11), 7237–7245. doi: 10.1002/2013JA019172
- 580 Johlander, A., Schwartz, S. J., Vaivads, A., Khotyaintsev, Y. V., Gingell, I., Peng,
 581 I. B., ... Burch, J. L. (2016). Rippled Quasiperpendicular Shock Observed by
 582 the Magnetospheric Multiscale Spacecraft. *Phys. Rev. Lett.*, *117*, 165101. doi:
 583 10.1103/PhysRevLett.117.165101
- 584 Kajdič, P., Raptis, S., Blanco-Cano, X., & Karlsson, T. (2021). Causes of jets in
 585 the quasi-perpendicular magnetosheath. *Geophysical Research Letters*, *48*(13),
 586 e2021GL093173. doi: 10.1029/2021GL093173
- 587 Karlsson, T., Kullen, A., Liljeblad, E., Brenning, N., Nilsson, H., Gunell, H., &
 588 Hamrin, M. (2015). On the origin of magnetosheath plasmoids and their rela-
 589 tion to magnetosheath jets. *Journal of Geophysical Research: Space Physics*,
 590 *120*, 7390–7403. doi: 10.1002/2015JA021487
- 591 Kennel, C. F., Edmiston, J. P., & Hada, T. (1985). A quarter century of collision-
 592 less shock research. In *Collisionless shocks in the heliosphere: A tutorial review*
 593 (p. 1-36). American Geophysical Union (AGU). doi: [https://doi.org/10.1029/
 594 GM034p0001](https://doi.org/10.1029/GM034p0001)
- 595 King, J. H., & Papitashvili, N. E. (2005). Solar wind spatial scales in and compar-
 596 isons of hourly Wind and ACE plasma and magnetic field data. *Jour-
 597 nal of Geophysical Research: Space Physics (19782012)*, *110*(A2). doi:
 598 10.1029/2004JA010649
- 599 Koller, F., Plaschke, F., Temmer, M., & Preisser, L. (2021). *THEMIS local and up-
 600 stream magnetosheath jet data 2008-2020*. <https://osf.io/6ywjz>.

- 601 Koller, F., Temmer, M., Preisser, L., Plaschke, F., Geyer, P., Jian, L. K., ... LaM-
602 oury, A. T. (2022). Magnetosheath Jet Occurrence Rate in Relation to
603 CMEs and SIRs. *Journal of Geophysical Research: Space Physics*, *127*(4),
604 e2021JA030124. doi: 10.1029/2021JA030124
- 605 LaMoury, A. T., Hietala, H., Plaschke, F., Vuorinen, L., & Eastwood, J. P. (2021).
606 Solar wind control of magnetosheath jet formation and propagation to the
607 magnetopause. *Journal of Geophysical Research: Space Physics*, *126*(9),
608 e2021JA029592. doi: 10.1029/2021JA029592
- 609 Lowe, R. E., & Burgess, D. (2003). The properties and causes of rippling in quasi-
610 perpendicular collisionless shock fronts. *Annales Geophysicae*, *21*(3), 671–679.
611 doi: 10.5194/angeo-21-671-2003
- 612 Madanian, H., Desai, M. I., Schwartz, S. J., Wilson, L. B., Fuselier, S. A., Burch,
613 J. L., ... Lindqvist, P.-A. (2021). The Dynamics of a High Mach Number
614 Quasi-perpendicular Shock: MMS Observations. *The Astrophysical Journal*,
615 *908*(1), 40. doi: 10.3847/1538-4357/abcb88
- 616 McFadden, J. P., Carlson, C. W., Larson, D., Ludlam, M., Abiad, R., Elliott,
617 B., ... Angelopoulos, V. (2008). The THEMIS ESA Plasma Instrument
618 and In-flight Calibration. *Space Science Reviews*, *141*(1-4), 277–302. doi:
619 10.1007/s11214-008-9440-2
- 620 Merka, J., Szabo, A., Slavin, J. A., & Peredo, M. (2005). Three-dimensional position
621 and shape of the bow shock and their variation with upstream Mach numbers
622 and interplanetary magnetic field orientation. *Journal of Geophysical Research:*
623 *Space Physics*, *110*(A4), 1–13. doi: 10.1029/2004JA010944
- 624 Omid, N., Desai, M., Russell, C. T., & Howes, G. G. (2021). High Mach Num-
625 ber Quasi-Perpendicular Shocks: Spatial Versus Temporal Structure. *Journal*
626 *of Geophysical Research: Space Physics*, *126*(9), e2021JA029287. doi: [https://](https://doi.org/10.1029/2021JA029287)
627 doi.org/10.1029/2021JA029287
- 628 Palmroth, M., Hietala, H., Plaschke, F., Archer, M., Karlsson, T., Blanco-Cano, X.,
629 ... Turc, L. (2018). Magnetosheath jet properties and evolution as determined
630 by a global hybrid-Vlasov simulation. *Annales Geophysicae*, *36*(5), 1171–1182.
631 doi: 10.5194/angeo-36-1171-2018
- 632 Petrukovich, A. A., & Chugunova, O. M. (2021). Detailed Structure of Very High-
633 β Earth Bow Shock. *Journal of Geophysical Research: Space Physics*, *126*(8),
634 e2020JA029004. doi: 10.1029/2020JA029004
- 635 Plaschke, F., Hietala, H., & Angelopoulos, V. (2013). Anti-sunward high-speed jets
636 in the subsolar magnetosheath. *Annales Geophysicae*, *31*(10), 1877–1889. doi:
637 10.5194/angeo-31-1877-2013
- 638 Plaschke, F., Hietala, H., Angelopoulos, V., & Nakamura, R. (2016). Geoeffective
639 jets impacting the magnetopause are very common. *Journal of Geophysical Re-*
640 *search A: Space Physics*, *121*(4), 3240–3253. doi: 10.1002/2016JA022534
- 641 Plaschke, F., Hietala, H., Archer, M., Blanco-Cano, X., Kajdič, P., Karlsson, T., ...
642 Sibeck, D. (2018). Jets Downstream of Collisionless Shocks. *Space Science*
643 *Reviews*, *214*(5), 81. doi: 10.1007/s11214-018-0516-3
- 644 Plaschke, F., Hietala, H., & Vörös, Z. (2020). Scale sizes of magnetosheath jets.
645 *Journal of Geophysical Research: Space Physics*, *125*(9), e2020JA027962. doi:
646 10.1029/2020JA027962
- 647 Pollock, C., Moore, T., Jacques, A., Burch, J., Gliese, U., Saito, Y., ... Zeuch, M.
648 (2016, Mar 01). Fast Plasma Investigation for Magnetospheric Multiscale.
649 *Space Science Reviews*, *199*(1), 331-406. doi: 10.1007/s11214-016-0245-4
- 650 Raptis, S., Karlsson, T., Plaschke, F., Kullen, A., & Lindqvist, P.-A. (2020).
651 Classifying Magnetosheath Jets Using MMS: Statistical Properties. *Jour-*
652 *nal of Geophysical Research: Space Physics*, *125*(11), e2019JA027754. doi:
653 10.1029/2019JA027754
- 654 Raptis, S., Karlsson, T., Vaivads, A., Pollock, C., Plaschke, F., Johlander, A., ...
655 Lindqvist, P.-A. (2022). Downstream high-speed plasma jet generation as a

- 656 direct consequence of shock reformation. *Nature Communications*, 13(1), 598.
 657 doi: 10.1038/s41467-022-28110-4
- 658 Russell, C. T., Anderson, B. J., Baumjohann, W., Bromund, K. R., Dearborn,
 659 D., Fischer, D., . . . Richter, I. (2016, Mar 01). The Magnetospheric Mul-
 660 tiscala Magnetometers. *Space Science Reviews*, 199(1), 189-256. doi:
 661 10.1007/s11214-014-0057-3
- 662 Schwartz, S. J. (1991). Magnetic field structures and related phenomena at quasi-
 663 parallel shocks. *Advances in Space Research*, 11(9), 231-240. doi: 10.1016/0273-
 664 -1177(91)90039-M
- 665 Shue, J.-H., Song, P., Russell, C. T., Steinberg, J. T., Chao, J. K., Zastenker, G., . . .
 666 Kawano, H. (1998). Magnetopause location under extreme solar wind condi-
 667 tions. *Journal of Geophysical Research: Space Physics*, 103(A8), 17691-17700.
 668 doi: 10.1029/98JA01103
- 669 Sulaiman, A. H., Masters, A., Dougherty, M. K., Burgess, D., Fujimoto, M., &
 670 Hospodarsky, G. B. (2015). Quasiperpendicular High Mach Number Shocks.
 671 *Phys. Rev. Lett.*, 115, 125001. doi: 10.1103/PhysRevLett.115.125001
- 672 Sundberg, T., Burgess, D., Scholer, M., Masters, A., & Sulaiman, A. H. (2017). The
 673 Dynamics of Very High Alfvén Mach Number Shocks in Space Plasmas. *The*
 674 *Astrophysical Journal Letters*, 836(1), L4. doi: 10.3847/2041-8213/836/1/L4
- 675 Suni, J., Palmroth, M., Turc, L., Battarbee, M., Johlander, A., Tarpus, V., . . .
 676 Zhou, H. (2021). Connection Between Foreshock Structures and the Genera-
 677 tion of Magnetosheath Jets: Vlasiator Results. *Geophysical Research Letters*,
 678 48(20), e2021GL095655. doi: 10.1029/2021GL095655
- 679 Tinoco-Arenas, A., Kajdič, P., Preisser, L., Blanco-Cano, X., Trotta, D., & Burgess,
 680 D. (2022). Parametric Study of Magnetosheath Jets in 2D Local Hy-
 681 brid Simulations. *Frontiers in Astronomy and Space Sciences*, 9. doi:
 682 10.3389/fspas.2022.793195
- 683 Vokhmyanin, M. V., Stepanov, N. A., & Sergeev, V. A. (2019). On the evalua-
 684 tion of data quality in the omni interplanetary magnetic field database. *Space*
 685 *Weather*, 17(3), 476-486. doi: <https://doi.org/10.1029/2018SW002113>
- 686 Vuorinen, L., Hietala, H., & Plaschke, F. (2019). Jets in the magnetosheath: IMF
 687 control of where they occur. *Annales Geophysicae*, 37(4), 689-697. doi: 10
 688 .5194/angeo-37-689-2019
- 689 Vuorinen, L., LaMoury, A. T., Hietala, H., & Koller, F. (submitted). *Magnetosheath*
 690 *jets over solar cycle 24: an empirical model*.
- 691 Walsh, B. M., Bhakyapaibul, T., & Zou, Y. (2019). Quantifying the uncertainty of
 692 using solar wind measurements for geospace inputs. *Journal of Geophysical Re-*
 693 *search: Space Physics*, 124(5), 3291-3302. doi: 10.1029/2019JA026507

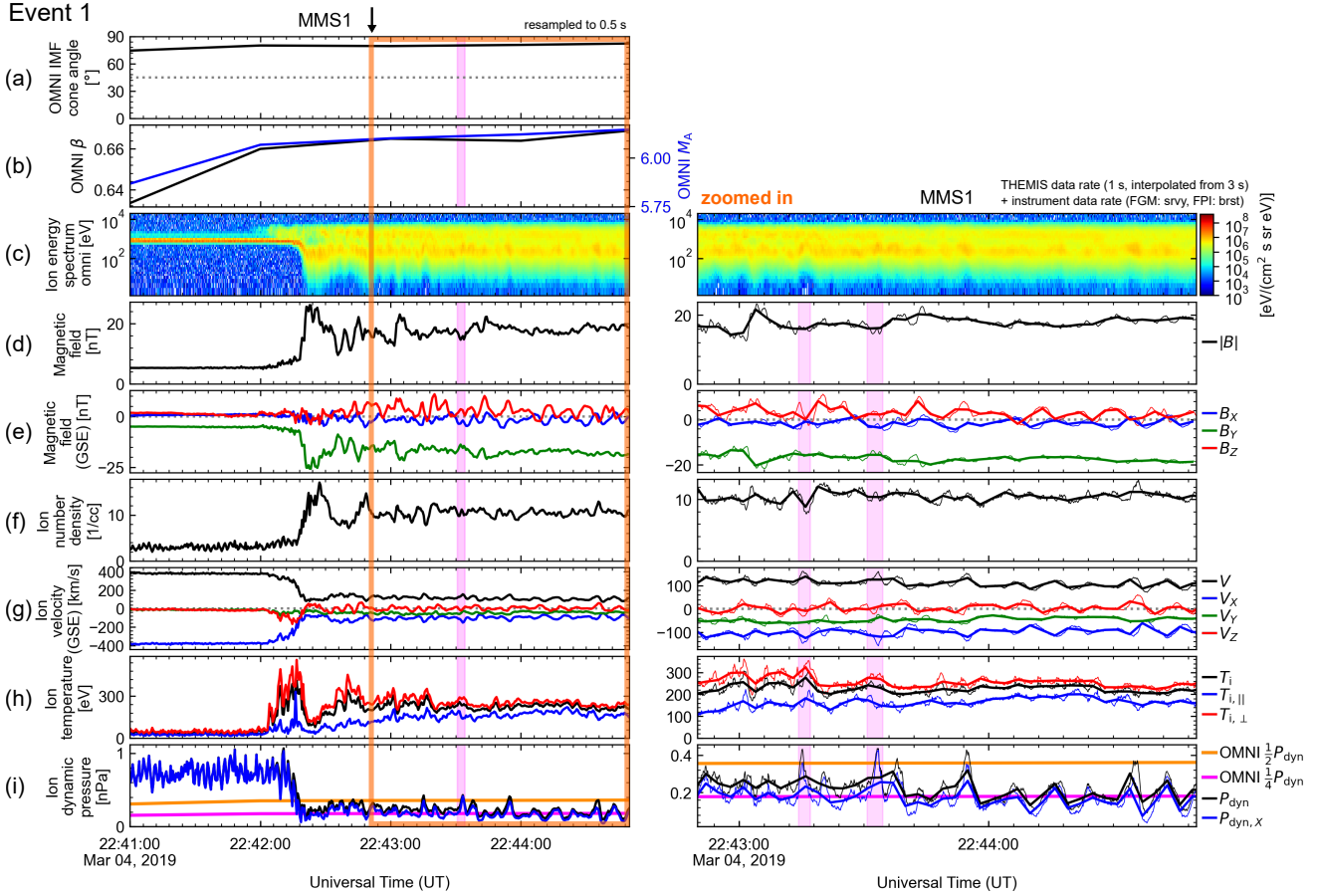


Figure 4. MMS1 observations on March 4, 2019 (Event 1). (a) OMNI IMF cone angle, (b) OMNI solar wind β and M_A , (c) ion omni-directional energy spectrogram, (d) magnetic field magnitude, (e) magnetic field GSE components, (f) ion number density, (g) ion velocity magnitude and GSE components, (h) ion total, parallel, and perpendicular temperatures, and (i) total and GSE $-X$ aligned dynamic pressures with 1/2 (orange) and 1/4 (magenta) of OMNI solar wind dynamic pressure. The magenta shading indicates a jet found using the Plaschke et al. (2013) jet criteria. The black arrow on top shows the selected upstream edge of the magnetosheath window in which we search for jets. In the left panel, the data are downsampled to 0.5 s cadence, and one jet is found with this cadence. In the zoomed-in panel on the right, thin lines show instrument resolution: survey mode for FGM and burst mode for FPI. Two jets were found using this FPI data. Thick lines show the data first downsampled to 3 s cadence and then interpolated to 1 s to be directly comparable to the statistical THEMIS data set. No jets were found using this data.

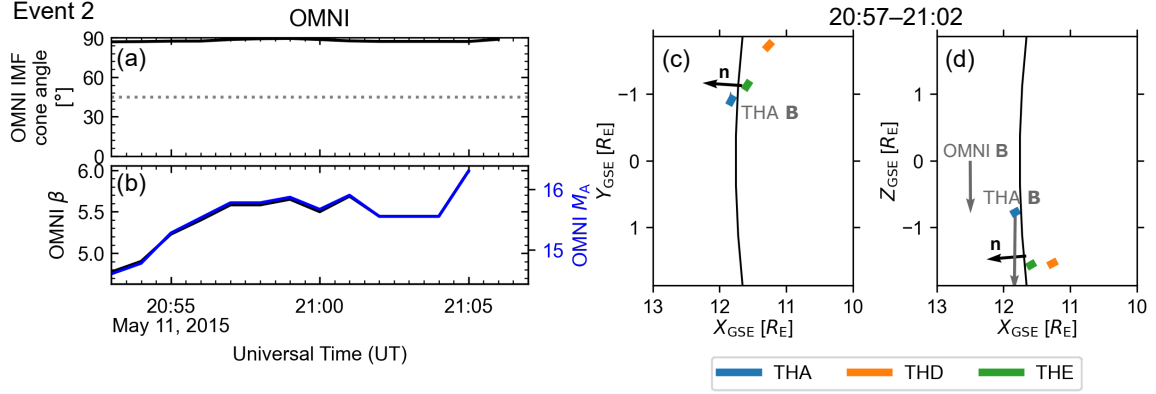


Figure 5. OMNI measurements for Event 2 on May 11, 2015: (a) IMF cone angle, (b) β and M_A . The locations of THEMIS A, D, and E spacecraft during 20:57–21:02 UT in the GSE (c) X - Y plane and (d) X - Z plane. The black line represents a model bow shock (Merka et al., 2005). The black arrows represent the model bow shock normal vectors at the point closest to THEMIS E. Gray arrows represent the average magnetic field vectors observed by OMNI and THEMIS A in the solar wind.

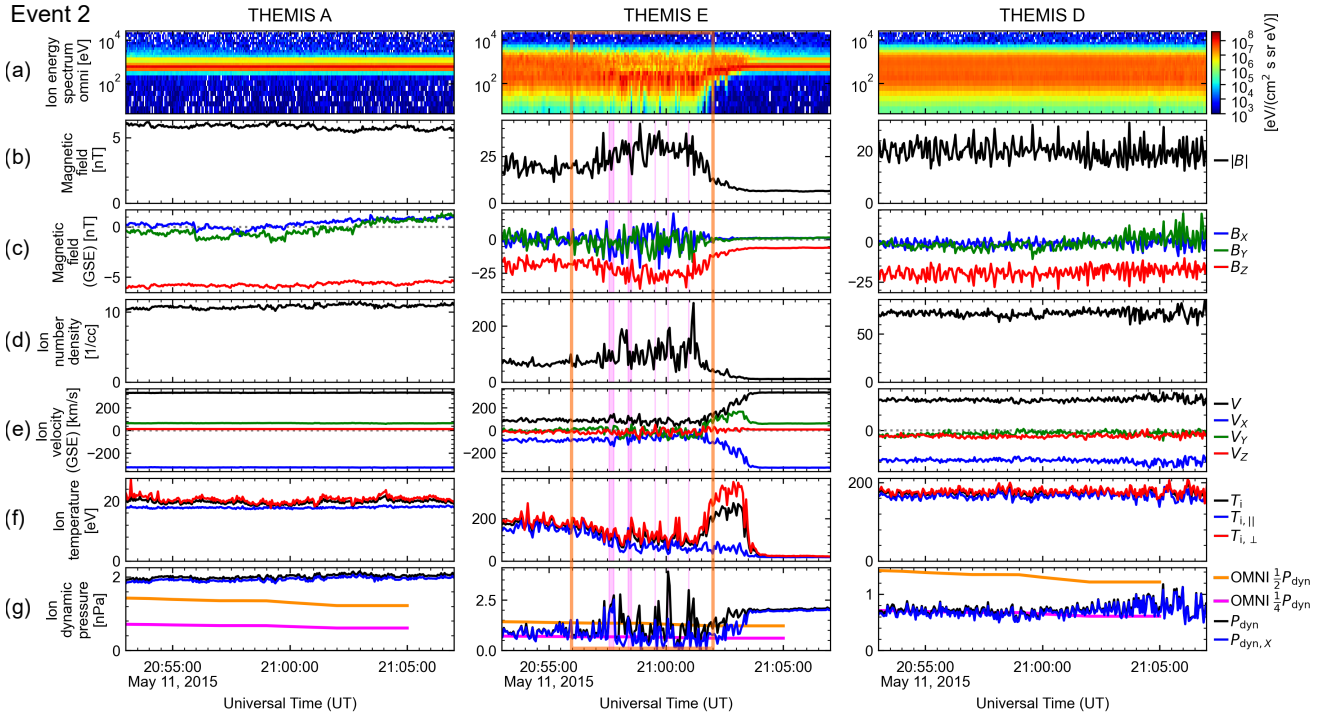


Figure 6. THEMIS A, E, and D observations for Event 2. (a) ion omni-directional energy spectrogram, (b) magnetic field magnitude, (c) magnetic field GSE components, (d) ion number density, (e) ion velocity magnitude and GSE components, (f) ion total, parallel, and perpendicular temperatures, and (g) total and GSE $-X$ aligned dynamic pressures with 1/2 (orange) and 1/4 (magenta) of OMNI solar wind dynamic pressure. The magenta shading indicates a jet found using the Plaschke et al. (2013) jet criterion on reduced level ESA data.

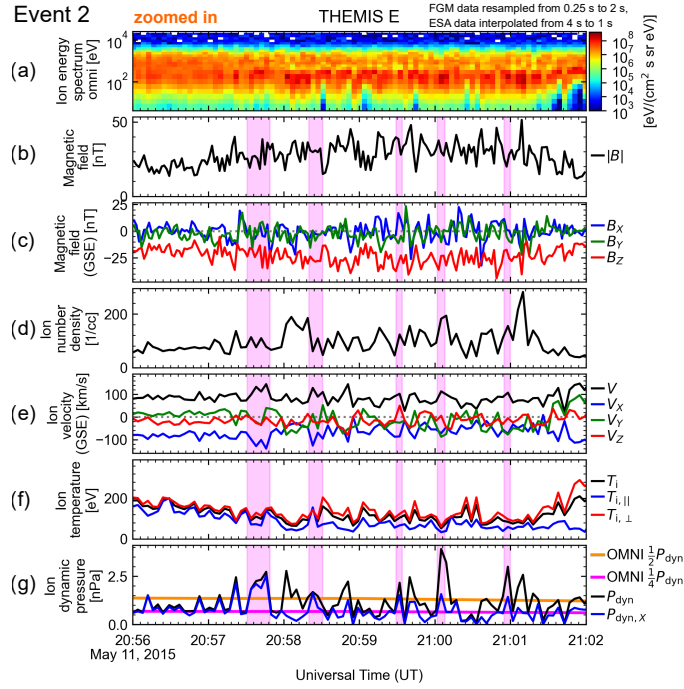


Figure 7. A zoom-in of THEMIS E observations for Event 2 in the same format as in Figure 6. The plasma data have been interpolated to 1 s cadence to match the cadence of the statistical data set. The magenta shading indicates a jet found using the Plaschke et al. (2013) jet criterion on this 1-s cadence data.

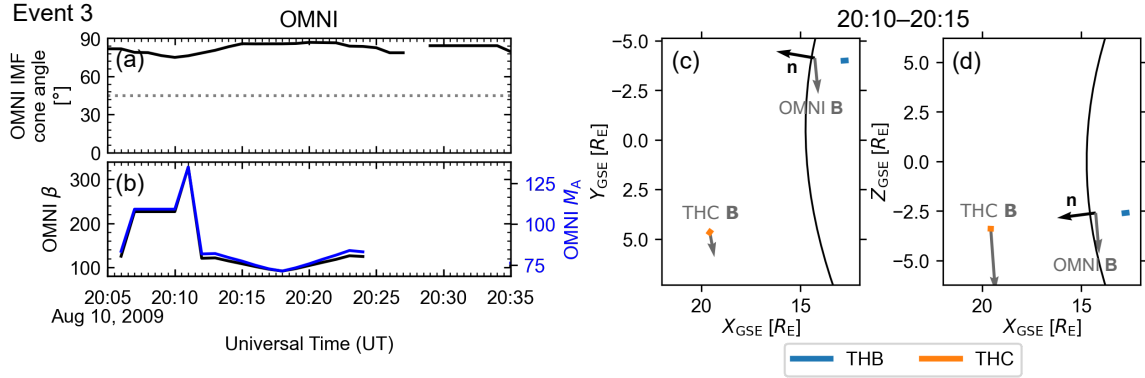


Figure 8. OMNI measurements for Event 3 on August 10, 2009: (a) IMF cone angle, (b) β and M_A . The locations of THEMIS B and C spacecraft during 20:10–20:15 UT in the GSE (c) X – Y plane and (d) X – Z plane. The black line represents a model bow shock (Merka et al., 2005) for reference, but the model is calculated for $B = 2$ nT that is larger than the observed value, as the model is not reliable for the observed values $B \lesssim 1$ nT. The black arrows represent the model bow shock normal vectors at the point closest to THEMIS B. Gray arrows represent the average magnetic field vectors observed by OMNI and THEMIS C in the solar wind.

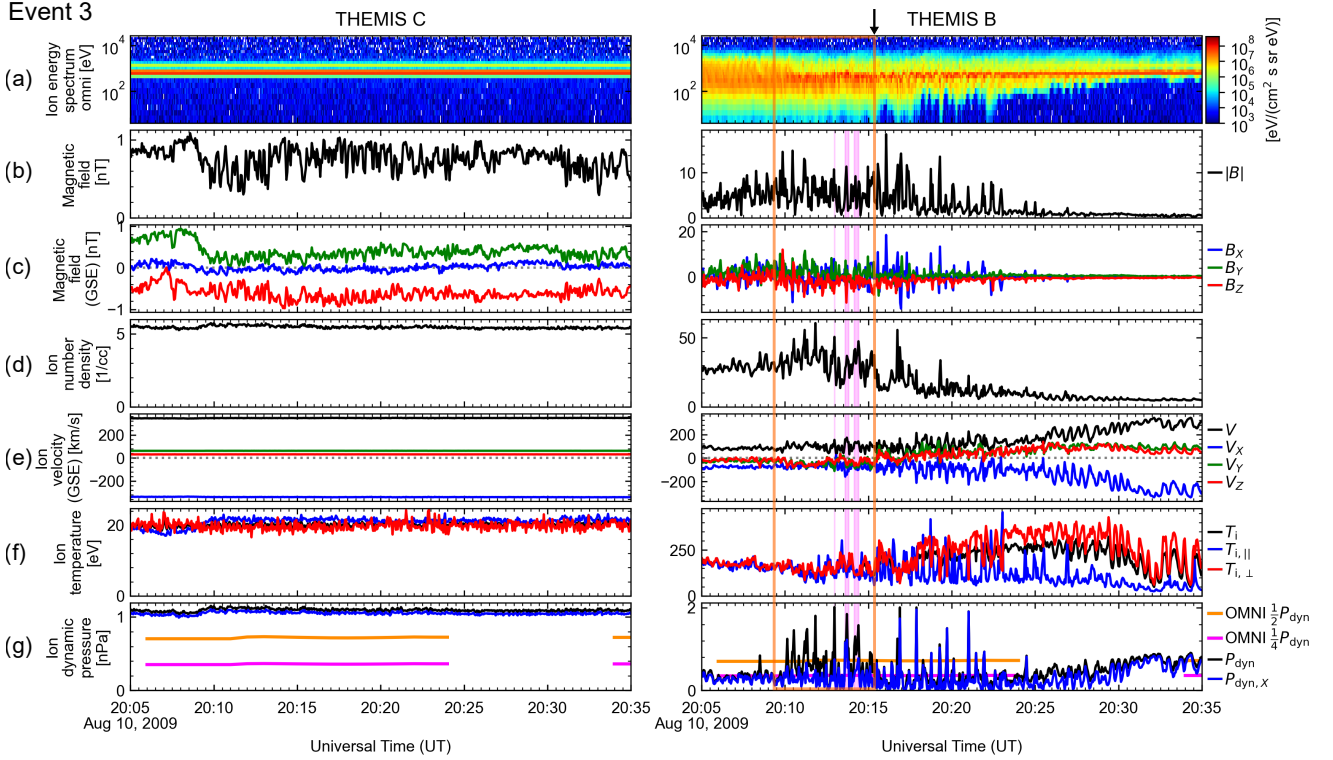


Figure 9. THEMIS C and B observations for Event 3 in the same format as in Figure 6. The magenta shading indicates a jet found using the Plaschke et al. (2013) jet criterion on the ESA reduced level data. The black arrow on top shows the selected upstream edge of the magnetosheath window in which we search for jets.

Event 4

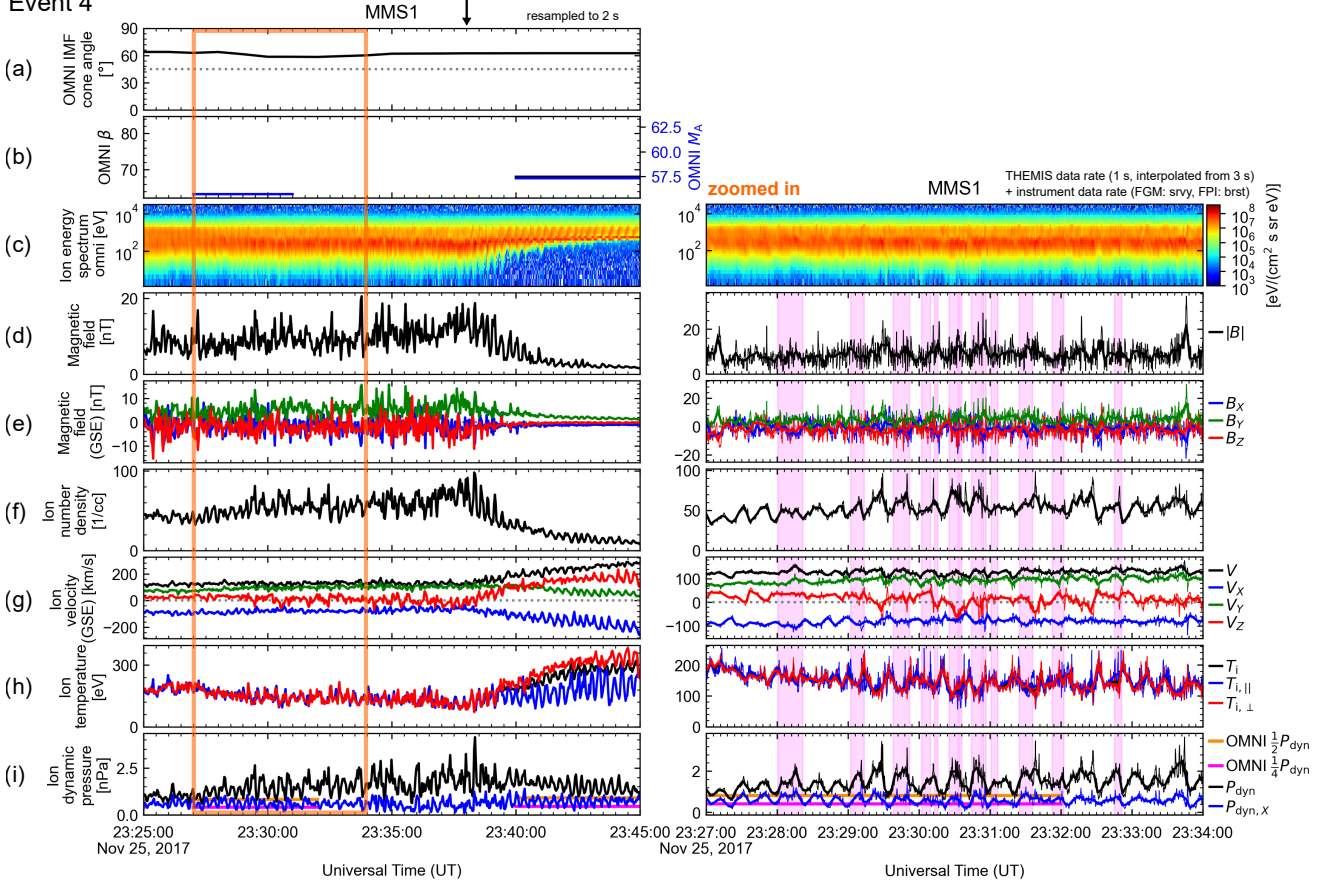


Figure 11. MMS1 crossing the Earth’s bow shock from the magnetosheath to the solar wind on November 25, 2017, (Event 4) in the same format as Figure 4. The black arrow on top shows the selected upstream edge of the magnetosheath window in which we search for jets. In the left panel, the data are downsampled to 2s cadence. No jets were found using this cadence. In the zoomed-in panel on the right, thin lines show instrument resolution data: survey mode for FGM and burst mode for FPI. Many jets were found using this data. Thick lines show data first downsampled to 3s cadence and then interpolated to 1s to be directly comparable to the statistical THEMIS data set. No jets were found when using this data.